Electronic Supplementary Material (ESI) for Nanoscale.

Supporting Information

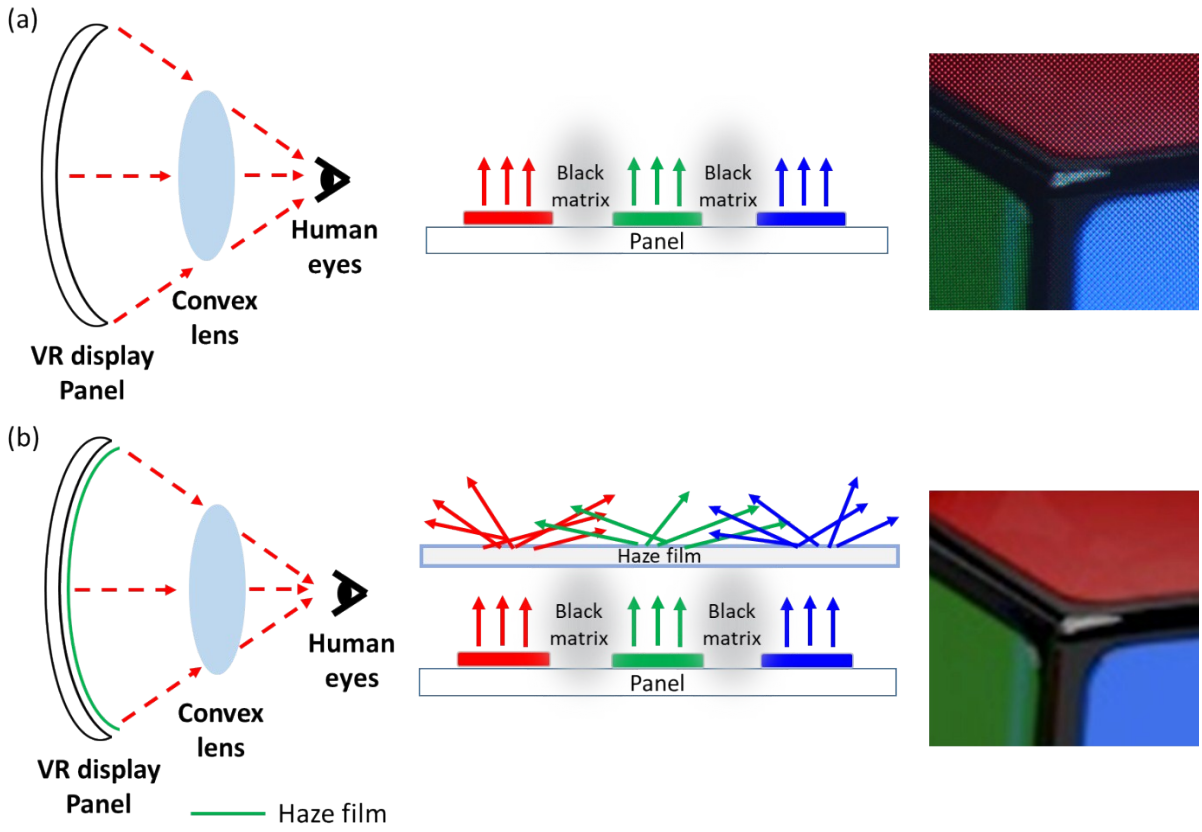

Fig. S1. Schematic of Screen-door effect in VR display: (a) VR without haze film, (b) VR with haze film. (Left: Components of VR headset, Middle: Propagation of the light from sub-pixels in VR panel, Right: Part of cube image through VR display)

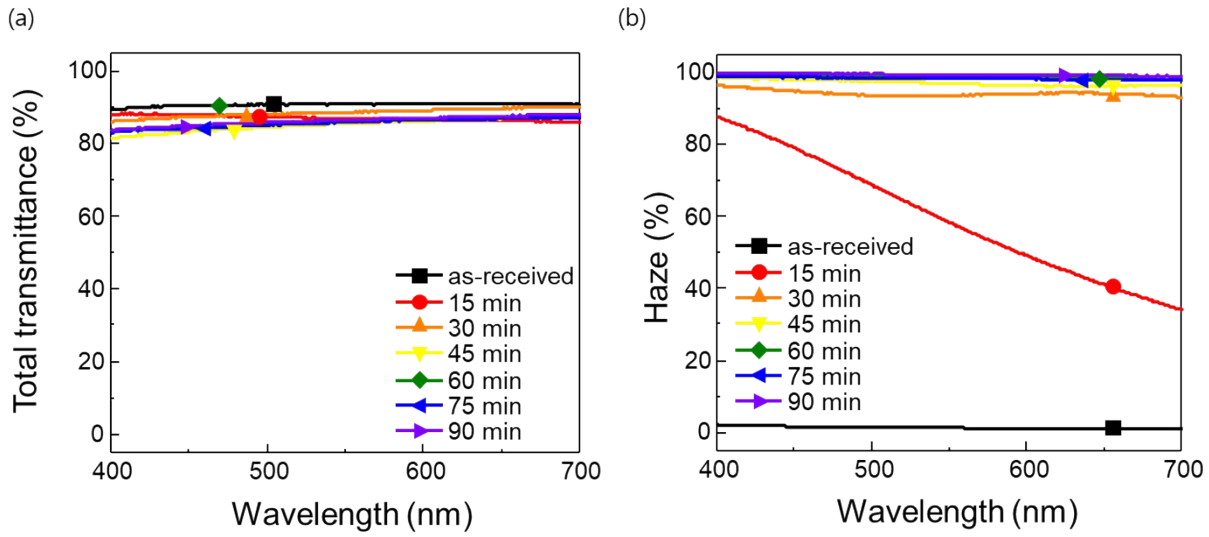

Fig. S2. Wavelength spectrums of the O_2 plasma treated PET with different plasma treatment time: (a) Total transmittance and (b) haze of O_2 plasma treated PET.

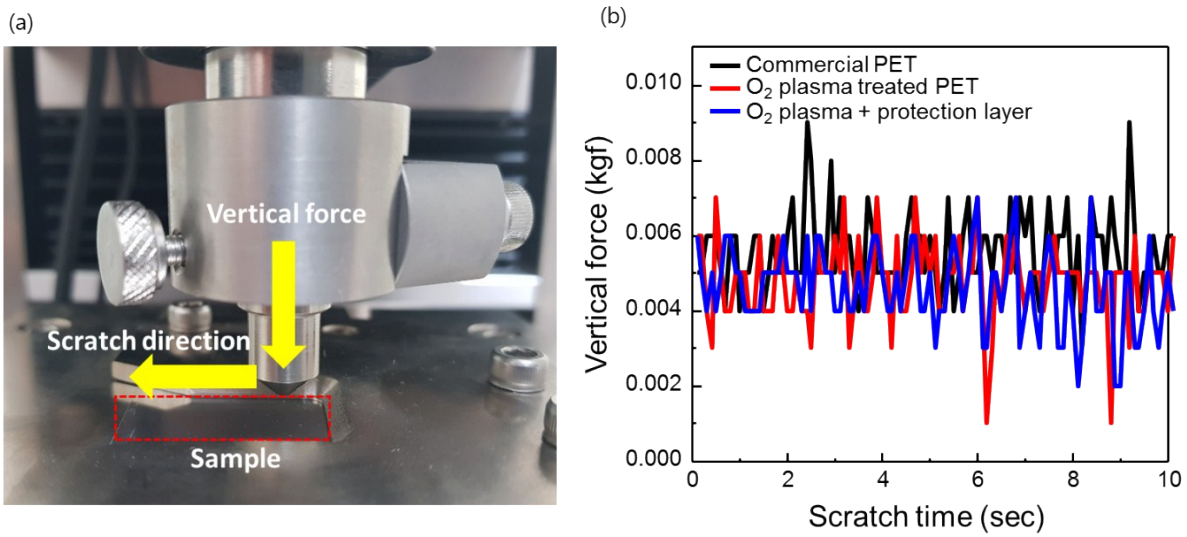

Fig. S3. (a) Photograph of scratch test on the PET film. (b) Results of scratch test on different flexible film.

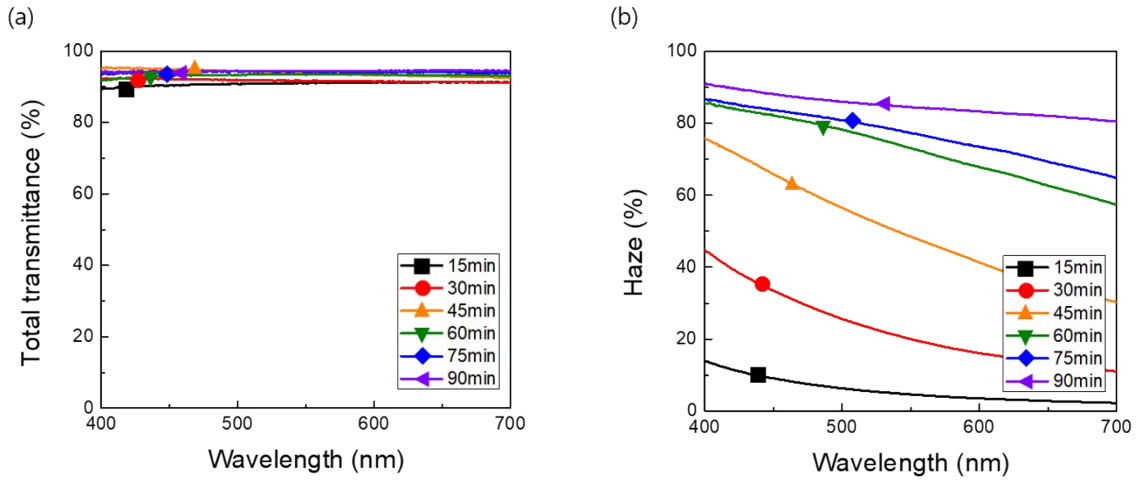

Fig. S4. Wavelength spectrums of the O_2 plasma treated PET coated with PDMS by different plasma treatment time: (a) Total transmittance and (b) haze of O_2 plasma treated PET.

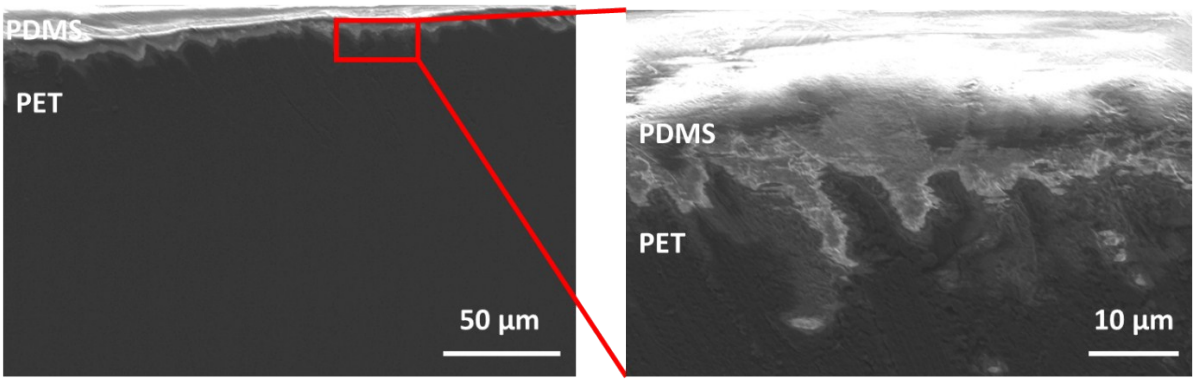

Fig. S5. Cross-sectional SEM image of hazy film cut by laser cutter (coated with PDMS as $R_{b/c}$=40)

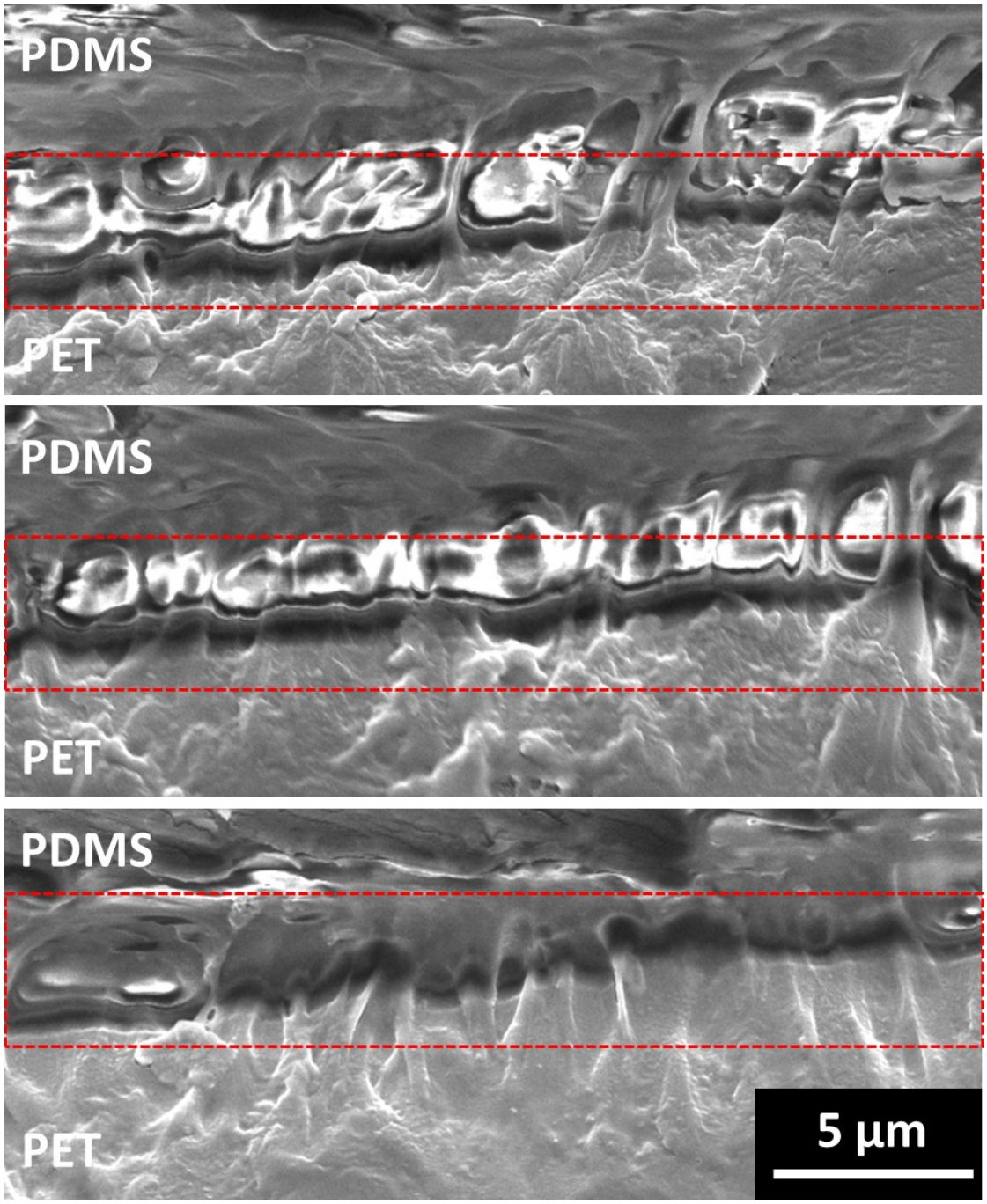

Fig. S6. Cross-sectional SEM image of hazy film cut by scissors (coated with PDMS as $R_{b/c}$=40)

Various methods were tried to cut the hazy film as well as to verify the existence of embedded air gaps. First, focused ion beam (FIB) method was conducted. In typical FIB, heavy metal ion (such as Ga^{2+}) is used as a source to cutting target materials, which induce a local heating at the irradiated surface during the preparation of sample. Only a few works related to reducing the FIB damages of soft materials are reported (*Microscopy Today*, **2009**, 17, 20,

Ultramicroscopy, **2011**, 111, 191). These works only prevent surface from damages and deformation, not the entire volume of materials from deformation. In this work, micro-sized air gaps were formed inside the film, so it was impossible to obtain a deformation-free image of air gaps and micropatterns due to the severe damages and deformation by the FIB process.

Second, laser cutting method was used. Since the laser has highly dense energy to cut the sample, the soft materials are easily deformed. Same as FIB, laser cutter was not suitable to investigate air gaps inside the film. Cross-sectional SEM images of films, cut by laser cutting methods, are shown in **Fig. S5**. The interface of PET/air/PDMS was melted by the heat from laser, thereby resulting in deformation of film. Thus, the cutting methods, which are using high energy, are not suitable for investigation of air gap inside the polymer film.

In our work, we cut the sample by typical cutter (such as knife, scissors) and took cross-sectional SEM images of air gap. We have tried many times to get better images and the best images are shown in **Fig. S6**. It was observed that a number of air gaps are captured at the valley of the flexible hazy substrate. Also the size of the air gaps were increased as the viscosity of the PDMS was increased. This observations is in good agreement with the RCWA simulation in **Fig. 6** of manuscript. Although the images of air gaps were somehow ambiguous, it is clear for the existence of the air gaps embedded into the substrate.

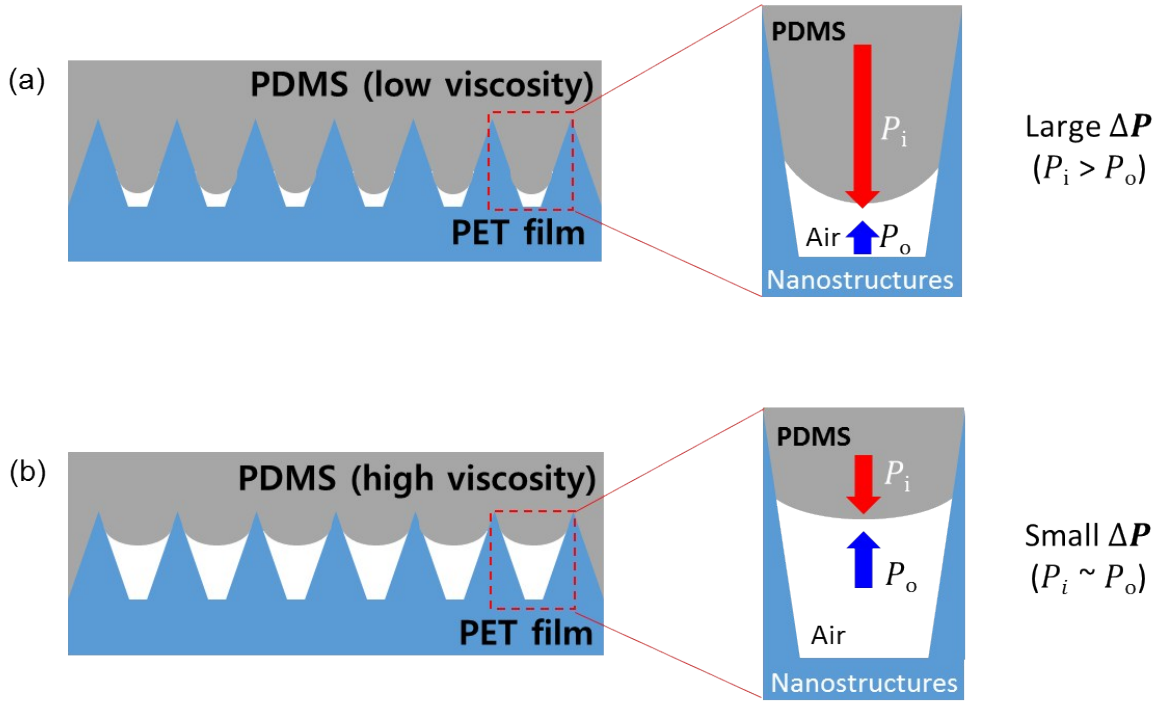

Fig. S7. Schematic illustrations of formation of air gap inside the hazy film with using low and high viscous PDMS for protection layer.

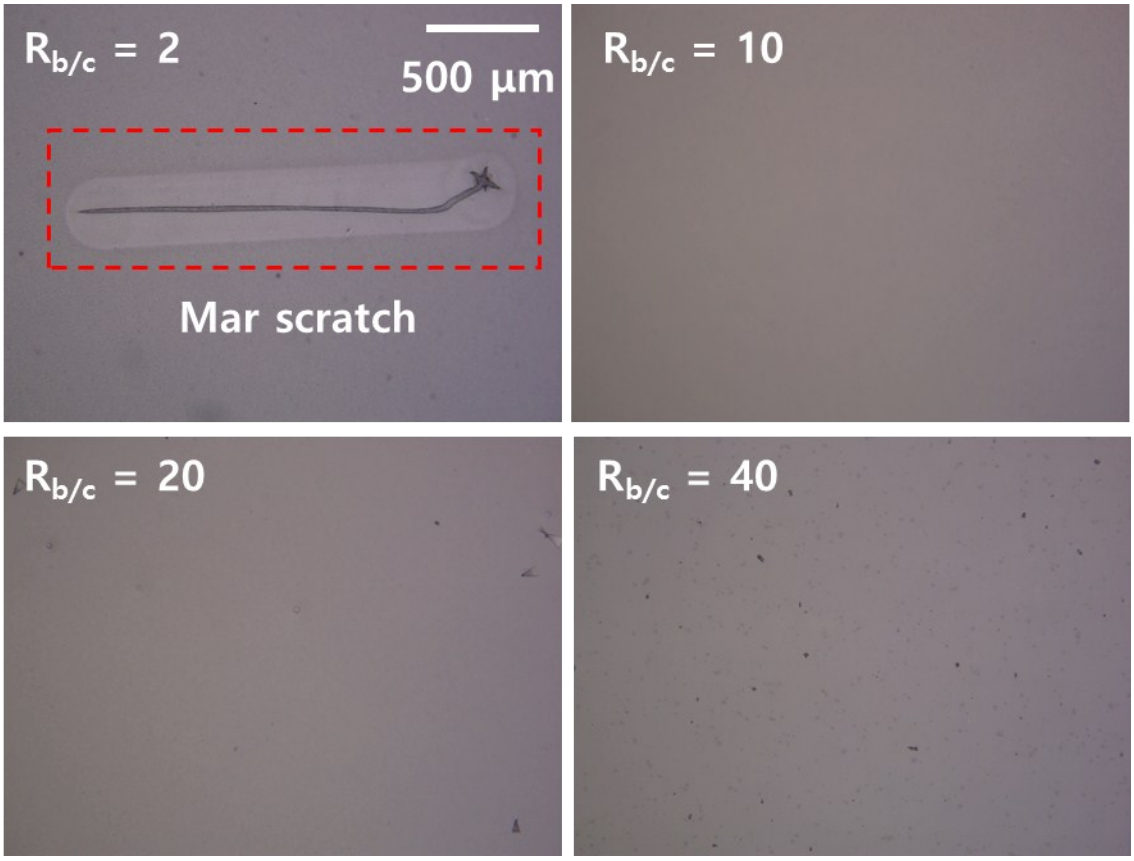

Fig. S8. Optical microscope images of hazy films after scratch test with using different $R_{b/c}$ of the PDMS.

Several literatures reported that the elastic modulus of PDMS network could be tuned linearly with the amount of the curing agent because the curing agent links the base polymer.[1, 2] The low $R_{b/c}$ produces a longer polymer chain in PDMS and the longer polymer chains have high Young's modulus and are vunerable to compressive force according to Hooke's law.[1,2] In order to experimentally confirm whether the Rb/c of the PDMS affected the scratch resistance, we performed the scratch test to **(Fig. S8)**. At $R_{b/c}$ = 2, the minor mar damage was observed on the PDMS. In contrast, there were no scratch-induced damages at $R_{b/c} \geq 10$. From these, the high $R_{b/c}$ could achieve not only the good mechanical stability, but also the excellent optical haze.

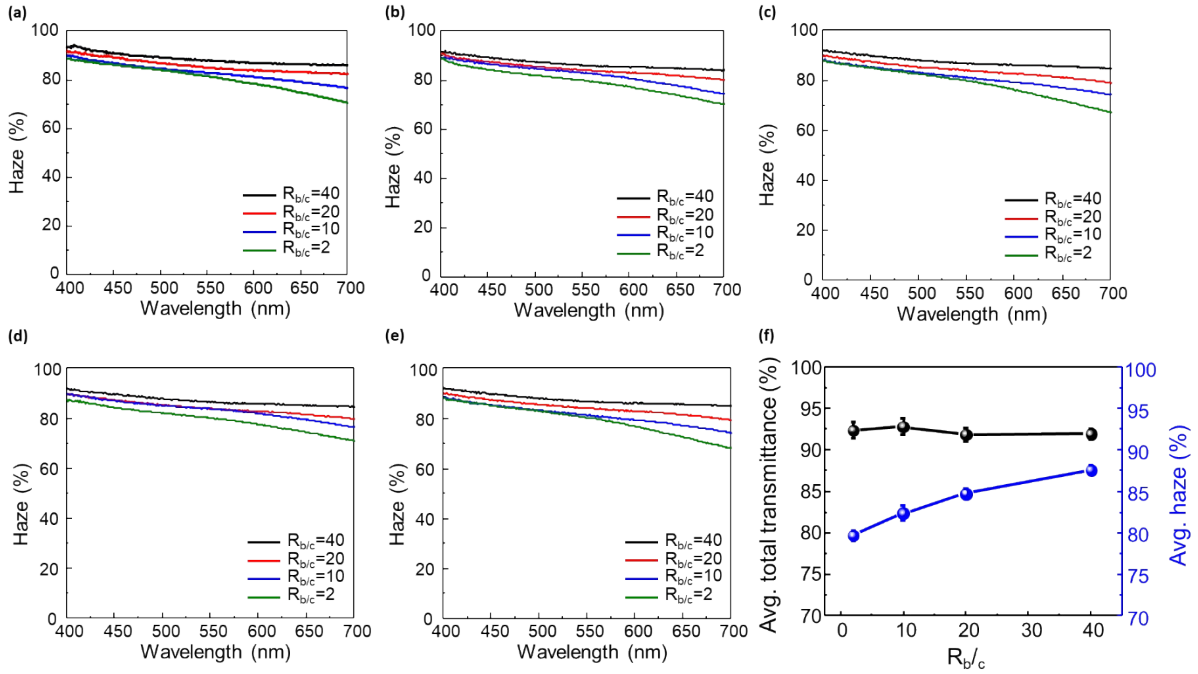

Fig. S9. Reliability test of flexible hazy films with different $R_{b/c}$: (a)~(e) the haze spectrums of hazy films, which are made 5 times in controlled condition, with different $R_{b/c}$. (f) Average optical properties of hazy films as a function of $R_{b/c}$.

We coated the PDMS on patterned PET with different $R_{b/c}$ for 5 times to clarify the uniformity and reliability. As shown in **Fig. S9**, the haze increased from 80 ±0.6 % to 88 ± 0.6 % as the $R_{b/c}$ increased meanwhile maintaining the total transmittance of 92 ± 0.9 %. The tendency of increment of haze by the $R_{b/c}$ showed the same for the hazy films, which are made 5 times in controlled condition. Thus, the size of the air gap could be tuned by the viscosity of the PDMS, resulting in control of the optical properties.

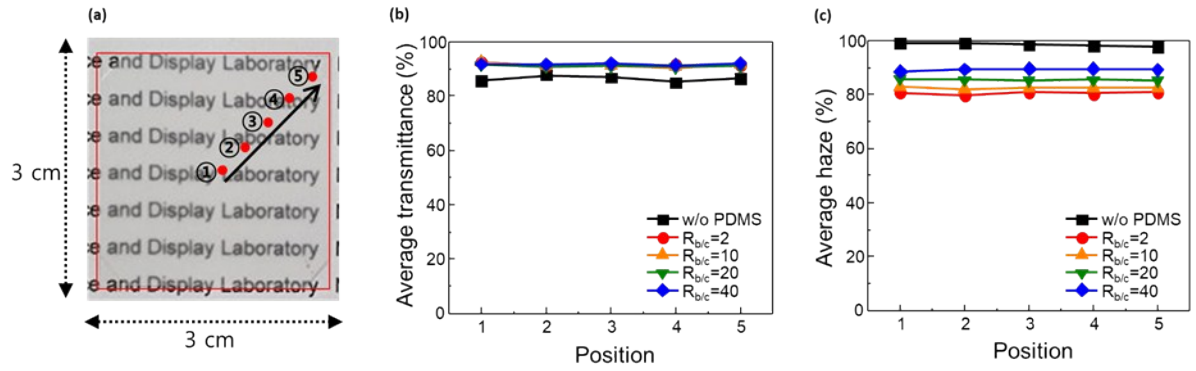

Fig. S10. (a) Schematic image of positions for measuring optical properties of hazy film. Measured optical properties of hazy film with different measured position: (b) Average total transmittance, (c) Average haze before and after coating the different PDMS.

We measured the optical properties of 90 min plasma-treated PET film at 5 points diagonally from the center **(Fig. S10)**. Before PDMS coating, the total transmittance showed average of 86.4% and standard deviation of 0.9 % and the haze showed average of 98.5% and standard deviation of 0.5 %. After PDMS coating, the total transmittance was as high as 91.7 $\pm$ 0.5 %. As the $R_{b/c}$ increases, the haze increased from 80.6 $\pm$ 0.4 % to 89.2 $\pm$ 0.3 %. All the hazy films showed the standard deviation of optical properties below 1 %. Thus, our hazy films exhibit very uniform optical properties over the entire area of film.

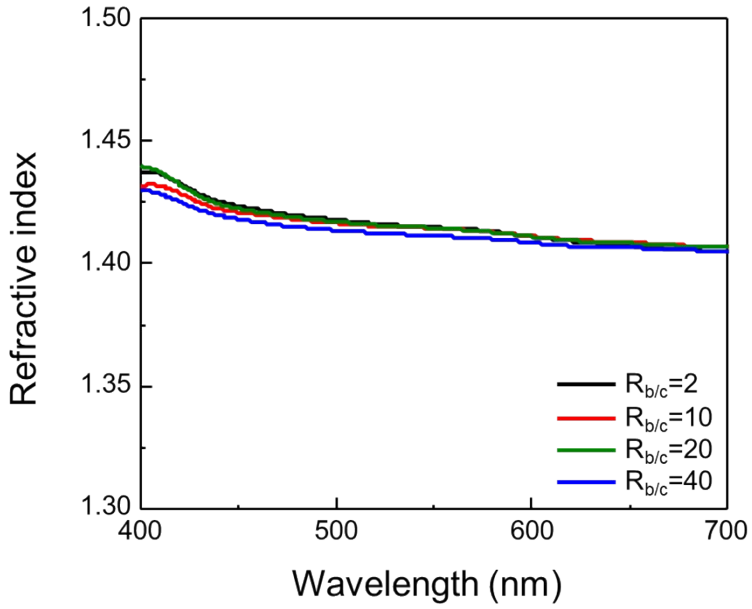

Fig. S11. Refractive index of PDMS with different $R_{b/c}$ as a function of wavelength.

We measured the RI of PDMS with different $R_{b/c}$ as a function of wavelength in **Fig. S11**. The average RIs of PDMS with different $R_{b/c}$ were almost same as 1.41 in visible wavelengths. The difference of RI between PDMS and PET film (RI = 1.6) is as small as 0.17, thereby leading to negligible scattering of the light. According to the RCWA simulation results in the main text, the average haze increased with the size of the air gap, which is consistent with the experimental results. These provide the evidence that the haze of our flexible hazy film is mainly induced by the air gap embedded inside the film rather than RI difference between PDMS and PET. Also, the size of the air gap is the key role to increase the haze while maintaining the high total transmittance.

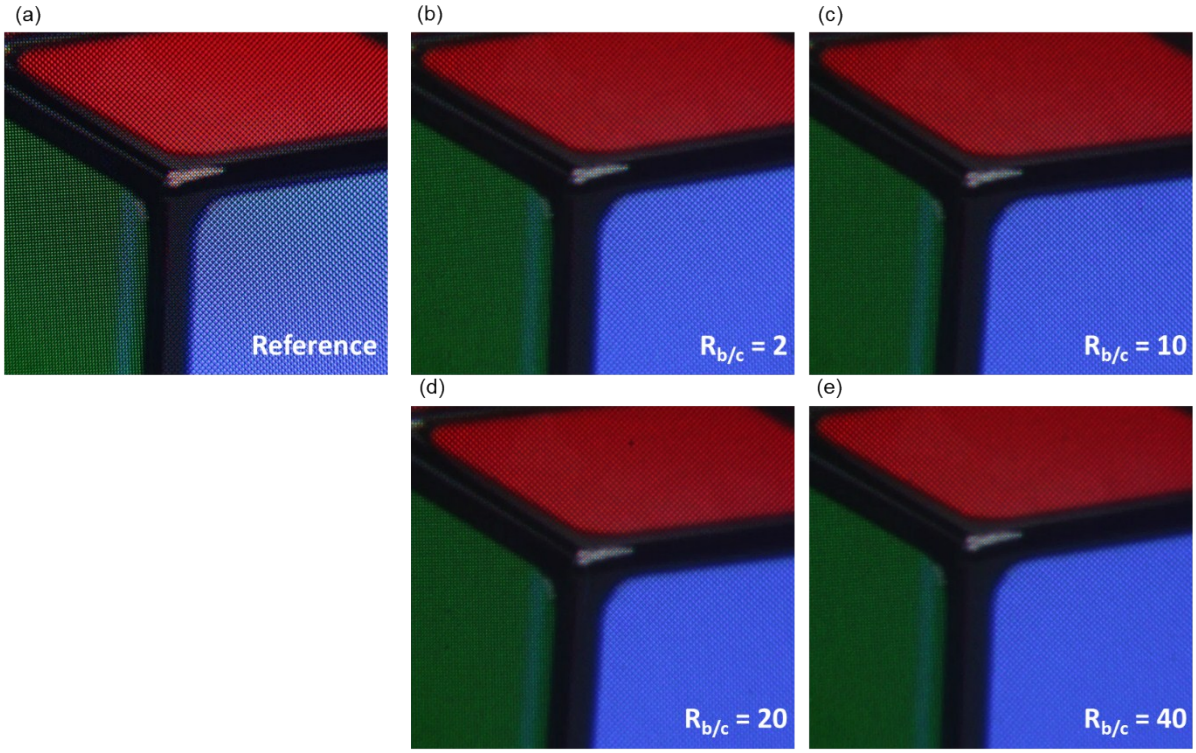

Fig. S12. VR images of the hazy films with using different $R_{b/c}$ of PDMS.

Name	Display type	Resolution
Playstation VR	5.7 inch OLED	1920 x 1080 (386 ppi)
Oculus Rift	3.5 inch OLED	1080 x 1200 (461 ppi)
HTC VIVE Pro	3.5 inch Dual AMOLED	1440 x 1600 (615 ppi)
Samsung Odyssey	3.5 inch Dual AMOLED	1440 x 1600 (615 ppi)
This work	6.1 inch Super AMOLED	2960 x 1440 (540 ppi)

Table S1. Summary of recent specification data of OLED VR display products.

	Red	Green	Blue
Reference	30.27 %	21.82 %	26.02 %
$R_{b/c}$ = 2	12.55 %	10.55 %	12.45 %
$R_{b/c}$ = 10	10.50 %	8.99 %	10.04 %
$R_{b/c}$ = 20	5.95 %	3.01 %	4.95 %
$R_{b/c}$ = 40	4.83 %	2.58 %	3.38 %

Table S2. SDE index calculation of hazy films coated with PDMS with different $R_{b/c}$.

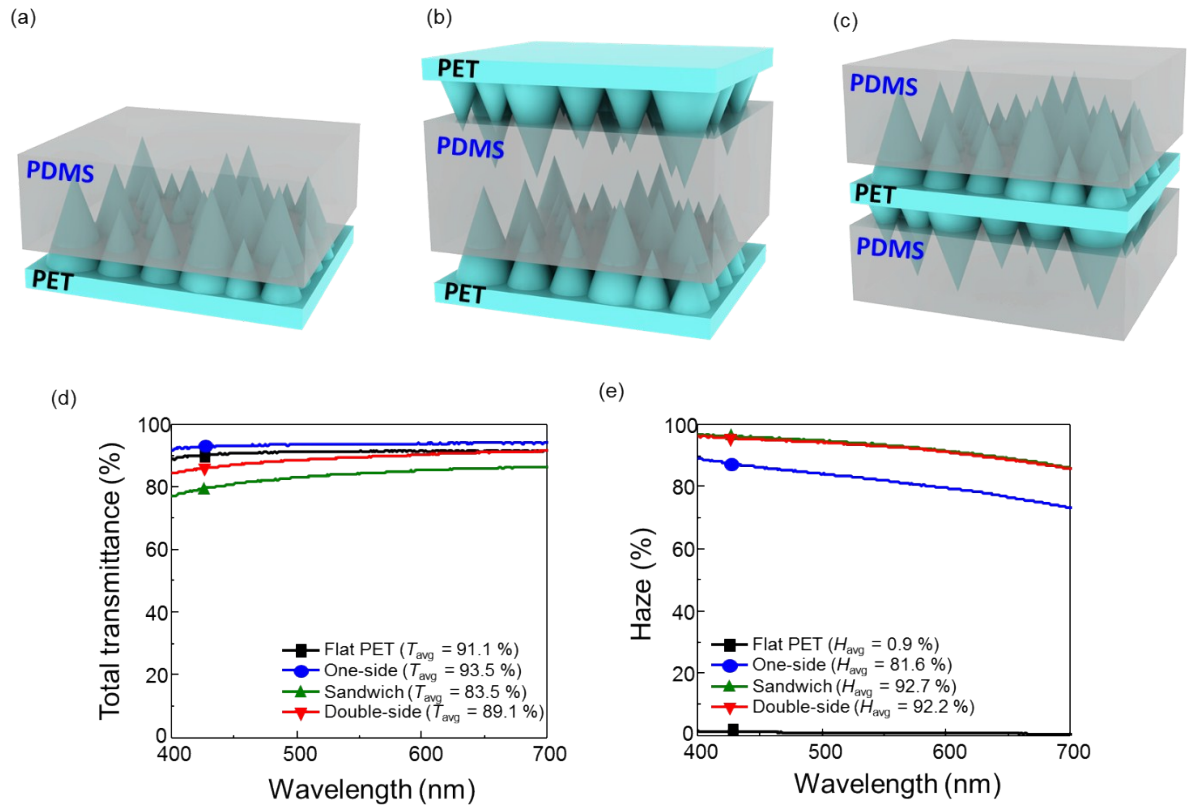

Fig. S13. Schematic illustration of hazy films with various structure design: (a) one-side patterned hazy film, (b) sandwich structured hazy film, and (c) double-side patterned hazy film. The optical properties of hazy films with various structure design: (d) Total transmittance, (e) haze.

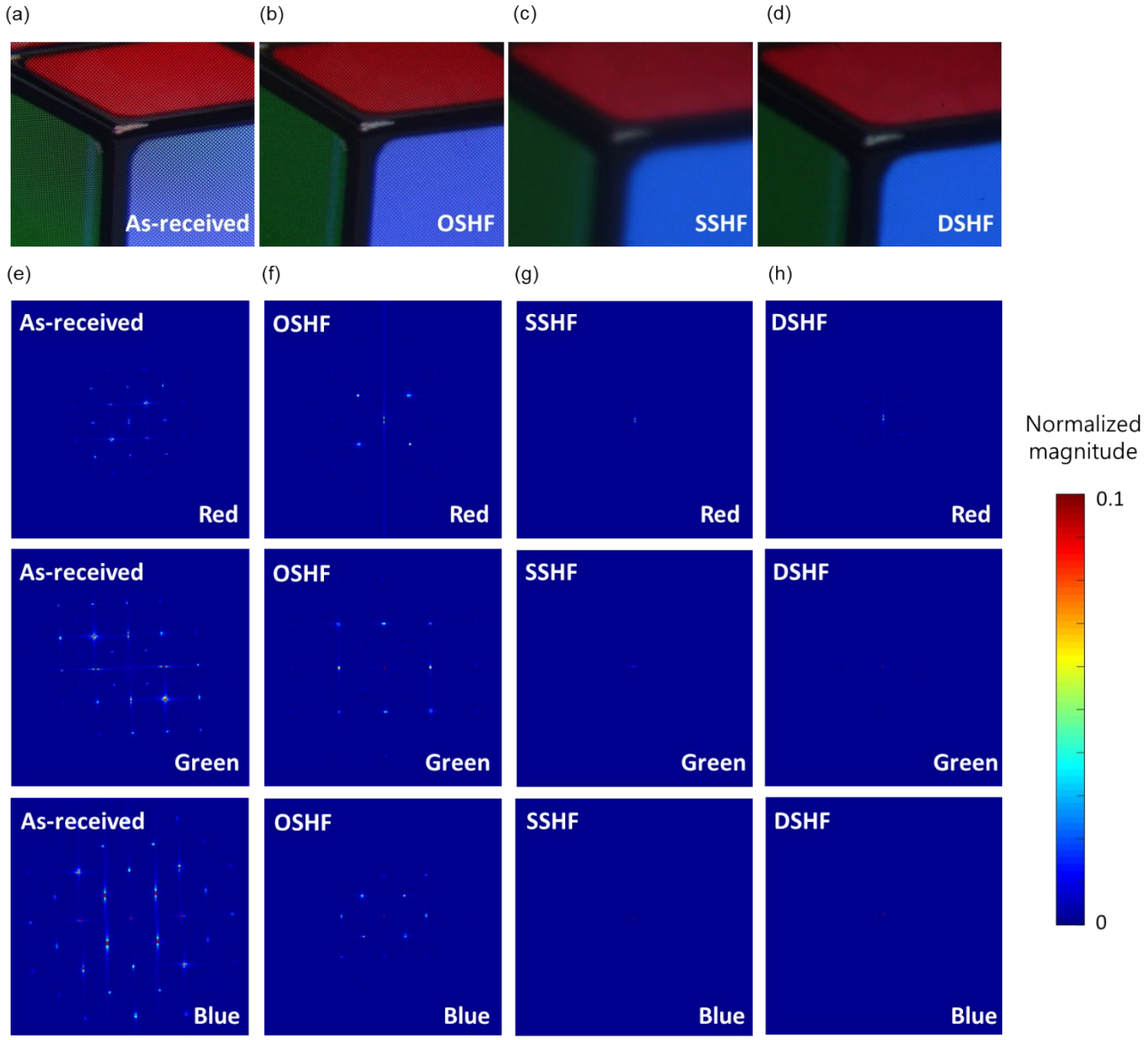

Fig. S14. VR images of the (a) as-received PET film (b) one-side patterned hazy film, (c) sandwich structured hazy film, and (d) double-side patterned hazy film. Fast Fourier transformed images with using the part of the full photographs in each colors: (e) As-received PET film, (f) one-side patterned hazy film, (g) sandwich structured hazy film, (h) double-side patterned hazy film.

	Red	Green	Blue
Reference	30.27 %	21.82 %	26.02 %
OSHF	10.50 %	8.99 %	10.05 %
SSHF	0.00 %	0.21 %	0.09 %
DSHF	2.09 %	0.50 %	0.47 %

Table S3. SDE index calculation of hazy films with different structure designs.

Design the structure of haze film for embedding more air bubbles

To embed more air bubbles, the flexible hazy films were made in different structures. The one-side patterned hazy film (OSHF) **(Fig. S13a)**, the sandwich structured hazy film (SSHF) **(Fig. S13b)**, and the double-side patterned hazy film (DSHF) **(Fig. S13c)** were used. The OSHF was made by PET with O_2 plasma treatment on the top of the surface of the PET; then coated with the PDMS. The SSHF was made by combining two patterned PETs with PDMS. The DSHF was made by PET with O_2 plasma treatment on both the top and the bottom surfaces of the PET; then, PDMS was coated on the both sides. To analyze only the impact of the architecture of the hazy film, the process condition of micro patterning on PET was fixed and the PDMS was used with $R_{b/c} = 10$. In **Fig. S13d-S13e**, the optical properties were measured with different structures of the hazy film. In case of OSHF, the total transmittance slightly increased all range of wavelength of visible light compared to the as-received PET because the air gaps induced the light scattering inside the hazy film, extracting trapped light from waveguide modes. The total transmittance of SSHF and DSHF was reduced by 83.5 % and 89.1 %, respectively, compared to OSHF. As the additional polymer

layer was placed in SSHF and DSHF compared to OSHF, the total internal reflection at the boundary of air and polymer substrate was more conducted, and it affected the reduction of transmittance. Since the number of air gap in SSHF and in DSHF were more than OSHF, the H_{avg} increased 10 % compared to OSHF about 92 %. The effect of light scattering from PET or PDMS could be excluded with the spectrum of as-received PET with PDMS coated sample. We could confirm that the air gap inside the film acted as a light scattering site, and the more air gaps, the more optical haze occurred.

Fig. S14, and **Table S3** in the Supporting Information show the VR applications of the hazy films with various structures. The optical haze was further increased by about 4 % by using the double-side patterned hazy film (DSHF), compared with one-side patterned hazy film (OSHF). The SDE index of DSHF was reduced about under 2 % for all colors. Therefore, the optical haze could be further improved by the design of the film to capture more air gaps, resulting in the reduction of SDE index.

Table S4. Summary of recent works related to the light scattering substrates (in visible wavelength (400~700 nm))

Substrate	Light scattering Methods	Scattering Center	Transmittance /Haze	Ref.
Glass	Hexagonal plate-shaped ZnO (Aerosol assisted CVD)	Outer	68.1% / 98.5%	3
	Monolithic fused silica nanograss (RIE etcing)	Outer	95.6% / 96.2%	4
	OTS/silica nanostructure (RIE etching)	Outer	91% / 98.1%	5
	Textured substrate (Chemical wet etching)	Outer	91.8% / 65.1%	6
	Corrugated substrate (Sn annealing and planarization layer)	Inner	~80% / 74.8%	7
	Polymer wrinkle structure (ZrO_2 planarization layer)	Inner	~85% / ~80%	8
	SiO_2 nanoparticles (Embedded in TiO_2 matrix)	Inner	76.9% / 20.3%	9
Paper	Ag nanowire (Lamination)	Outer	91% / 65%	10
PET	Substrate patterning (Plasma treatment)	Outer	89.4% / 95.5%	11
Tape	Aggregated AAO nanowire (Wet etching)	Outer	85% / 98%	12
PDMS	Pyramid-shaped patterning (Nano-imprinting)	Outer	75.5% / 80%	13
PDMS	SiO_2/polymer buckling (UVO treatment)	Outer	84% / 73%	14
PI	AgCl nanorod (Plasma-assisted growth)	Outer	50% / ~100%	15
PEN	Organic/Inorganic filler particle (PAI planarization layer)	Inner	85% / 43.4%	16
PS	Al_2O_3 nanoparticles (Spin-coating)	Inner	76.9% / 90.7%	17
PAI	BaO_4SrTi nanoparticle (Spin-coated with polymer solution)	Inner	52.7% / 96.6%	18

PET	Air-bubble (Pre-patterning and protection)	Inner	91.7% / 88.6%	This work

Recent works on the light scattering substrate are summarized in **Table S3.** In a VR headset, lenses magnify a two-dimensional display to an immersive 3D image. The shape of VR display panel is curved to realize high-quality 3D image. Due to the flexion of display panel, the hazy substrate should be flexible to reduce SDE in VR display. Thus, plastic substrates, which are more flexible and bendable than glass substrate, are more practical for VR displays.

The methods to make hazy plastic film could be classified into two parts; scattering center outside the film and scattering center embedded in the film **(Table S3)**. The scattering center outside the film composed of patterned surface or micro-lens array placed to the surface of the film. Although the haze is sufficiently high without reduction of transmittance, the patterned surface could be easily damaged and scratched. On the other hand, the scattering center embedded in the film could be protected by covering layer and thus has a good scratch resistance from external environment. Previously, scattering center embedded polymer film was demonstrated by adopting a low refractive index (RI) film and high RI nanoparticles. However, the transmittance of the film was degraded due to the Fresnel reflection induced by the high RI nanoparticles. In this work, the spontaneously produced air gaps, placed in between the pre-patterned plastic film and the protection layer, act as a scattering center. Since the air gaps have low RI, it is very effective for suppressing the Fresnel reflection when combined with polymer film (high RI). As a result, both high transmittance over 90 % and high hazy over 80 % could be demonstrated, leading to suitable application for SDE reduction in VR.

References

1. Z. Wang, A. A. Volinsky, N. D. Gallant, *J. Appl. Polym. Sci.*, 2014, **131**, 41050

2. S. H. Jeong, S. Zhang, K. Hjort, J. Hilborn and Z. Wu, *Adv. Mater.*, 2016, **28**, 5830-5836.

3. S. Chen, M. McLachlan, A. Sapelkin, and R. Binions, *J. Mater. Chem. A*, 2015, **3**, 22311

4. S. Haghanifar, T. Gao, R. T. R. De Vecchis, B. Pafchek, T. D. B. Jacobs, and P. W. Leu, *Optica*, 2017, **4**, 12, 1522

5. S. Haghanifar, P. Lu, M. I. Kayes, S. Tan, K. Kim, T. Gao, P. Ohodnicki, and P. W. Leu, *J. Mater. Chem. C*, 2018, **6**, 9191

6. S. Q. Hussain, A. H. T. Le, K. Mallem, H. Park, M. Ju, S. Lee, J. Cho, Y. Lee, J. Park, E.

Cho, Y. Lee, Y. Kim, and J. Yi, *Solar Energy*, 2018, **173**, 1173-1180

7. Y. H. Kim, J. Lee, W. M. Kim, C. Fuchs, S. Hofmann, H. Chang, M. C. Gather, L. Muller-Meskamp, and Karl Leo, *Adv. Funct. Mater.*, 2014, **24**, 2553-2559

8. H. Cho, E. Kim. J. Moon, C. W. Joo, E. Kim, S. K. Park, J. Lee, B. Yu, J. Lee, S. Yoo, and N. S. Cho, *Org. Electron.*, 2017, **46**, 139-144

9. J. Lee, Y. Y. Kwon, E. –H. Choi, J. Park, H. Yoon, and H. Kim, *Opt. Express*, 2014, **22**, A705-A714

10. C. Preston, Z. Fang, J. Murray, H. Zhu, J. Dai, J. N. Munday, and L. Hu, *J. Mater. Chem. C*, 2014, **2**, 1248

11. I. Lee, J. Y. Park, S. Gim, J. Ham, J. H. Son, J.-L. Lee, *Small*. 2015, **11**, 4480.

12. G. Kang, K. Bae, M. Nam, D. –H. Ko, K. Kim, and W. J. Padilla, *Energy Environ. Sci.*, 2015, **8**, 2650-2656

13. J. Ham, W. J. Dong, J. Y. Park, C. J. Yoo, I. Lee and J. L. Lee, *Adv. Mater.*, 2015, **27**, 4027-4033.

14. Y. Huang, Y. Liu, K. Youssef, K. Tong, Y. Tian, and Q. Pei, *Adv. Opt. Mater.*, 2018, **6**, 1801015

15. J. Y. Park, I. Lee, J. Ham, S. Gim, and J. –L. Lee, *Nat. Commun.*, 2017, **8**, 15650

16. E. Kim, H. Cho, K. Kim, T.-W. Koh, J. Chung, J. Lee, Y. Park, and S. Yoo, *Adv. Mater.*, 2015, **27**, 1624-1631

17. C.-H. Shin, E. Y. Shin, M.-H. Kim, J.-H. Lee and Y. Choi, *Opt. Express*, 2015, **23**, A133-A139.

18. K. Tong, X. Liu, F. Zhao, D. Chen and Q. Pei, *Adv. Opt. Mater.*, 2017, **5**, 1700307.